Optical Properties of $SrTiO_3$ under Applied Stress and Electric Field

R. C. CASELLA
National Bureau of Standards, Washington, D. C.
(Received 18 July 1966; revised manuscript received 22 September 1966)

Motivated by recent experiments on the effects of uniaxial stress on the superconducting transition and normal-state transport properties of $SrTiO_3$, we have carried out a symmetry analysis, obtaining the perturbed band structure and optical selection rules for the cases of uniaxial stress along the [111] and [001] axes and of static electric field along [001]. A comparison of the last case with $BaTiO_3$ in the C_{4v} ferroelectric phase suggests a model with a reversal in the order of the valence bands in $SrTiO_3$ relative to that proposed earlier. Selection rules for polarized light are obtained for both models and criteria for deciding experimentally which is correct are stated. An example is given of how the sign of the relative energy shift of the conduction valleys with stress may be determined optically.

I. INTRODUCTION

RECENTLY, Schooley[1] has observed a decrease in the superconducting transition temperature of strontium titanate with application of uniaxial stress along the [100] and [110] directions, observing no appreciable effect for the case of [111] stress. He interprets his results in terms of Cohen's[2] many-valley theory as an imbalance of valley populations for the cases of [100] and [110] stress with a consequent decrease in the BCS[3] parameter N(0)V, generated, in Cohen's interpretation, by intervalley electron-phonon interactions. The approximate null effect for stress in the [111] direction is in accord with the prediction of Kahn and Leyendecker[4] that the conduction-band minima lie along the ⟨100⟩ axes, probably at the Brillouin-zone edge, and the experimental findings of Frederikse, Thurber, and Hosler[5] based upon normal-state transport measurements. Moreover, Tufte and Stelzer[6] have observed ~10% effects on the normal resistive properties of $SrTiO_3$ due to applied uniaxial stress.

Since it would be interesting to correlate the experimental results discussed above with optical measurements at the fundamental edge, we have made a theoretical study of the effects of applied [111] and [001] uniaxial stress and [001] static electric field on the band structure, and the optical selection rules for $SrTiO_3$ in this region of the spectrum. Our results for the band structure along the cubic axes and for the optical selection rules with polarized light under the various perturbations are presented in Sec. II. We omit a discussion of the well-known group-theoretical techniques employed, but refer to excellent review articles.[7] Since we begin our analysis using the band structure calculated in Ref. 4 for cubic $SrTiO_3$ neglecting spin-orbit interaction, Sec. II also includes a discussion of the spin effects as well as natural deviations from the cubic lattice in the absence of applied perturbations, citing experimental evidence where necessary to estimate their magnitudes. We appeal to experiment once again in Sec. II to support our assumption of C_{4v} symmetry for $SrTiO_3$ in the presence of a strong electric field along the [001] axis.

In Sec. III, two examples are discussed of the application of our results to possible future experiments in the light of presently available optical evidence on unstrained crystals: Cardona[8] has examined the spectrum via reflectivity over an extensive range of photon energies (3–22 eV) and via refractive-index measurements below 3 eV. Recently, Blunt and Cohen[9] made transmission measurements near the fundamental edge over a range of absorption coefficients α from 10^{-2} to 10^3 cm^{-1} and temperatures from 4°K to room temperature. They find the well-known Urbach rule obeyed throughout with all lines converging to 3.37 eV in a plot of $\ln\alpha$ versus photon energy.

Given each of the two models postulated in Sec. III, together with additional stated assumptions about the nature of the critical points involved in the optical transitions, predictions are made for the results of experiments using polarized light with various applied perturbations on the crystals. These are stated in Sec. III and means of distinguishing between the models are again highlighted in the summary, Sec. IV. In the first model considered in Sec. III, the unperturbed band picture is taken from Ref. 4, whereas the second has a revised valence-band structure. Indirect experimental evidence motivating the assumption of the second model is also discussed in Sec. III.

The effect of exciton formation on the optical selection rules is ignored in our analysis. Because of the

[1] J. F. Schooley (private communication). To be presented at the Eighth International Conference on the Physics of Semiconductors, Kyoto (1966).
[2] M. L. Cohen, Phys. Rev. **124**, A511 (1964).
[3] J. Bardeen, L. Cooper, and J. R. Schrieffer, Phys. Rev. **108**, 1175 (1956).
[4] A. H. Kahn and A. J. Leyendecker, Phys. Rev. **135**, A1321 (1964). Also, A. H. Kahn (private communication).
[5] H. P. R. Frederikse, W. R. Thurber, and W. R. Hosler, Phys. Rev. **134**, A442 (1964); **143**, 648 (1966). Also, H. P. R. Frederikse (private communication).
[6] O. N. Tufte and E. L. Stelzer, Phys. Rev. **141**, 675 (1966).
[7] G. F. Koster, Solid State Phys. **5**, 173 (1957); R. S. Knox and A. Gold, *Symmetry in the Solid State* (W. A. Benjamin, Inc., New York, 1964); and V. Dvorak, Phys. Status Solidi **3**, 2235 (1963). See also Refs. 24, 25, and 26.
[8] M. Cardona, Phys. Rev. **140**, A651 (1965).
[9] R. F. Blunt and M. I. Cohen (private communication). See also L. H. Grabner, M. I. Cohen, and R. F. Blunt, Bull. Am. Phys. Soc. **11**, 86 (1966).

TABLE I. Optical selection rules for direct transitions in electric-dipole approximation. The c axis is chosen to be the axis of applied stress or static electric field. $\mathbf{E}$ denotes the polarized radiation electric field.

(a) Cubic crystal		(b) [111] Stress		(c) [001] Stress			(d) [001] Static electric field		
Allowed	Forbidden	Allowed $\mathbf{E}\perp c$	Allowed $\mathbf{E}\parallel c$	Allowed $\mathbf{E}\perp c$	Allowed $\mathbf{E}\parallel c$	Forbidden	Allowed $\mathbf{E}\perp c$	Allowed $\mathbf{E}\parallel c$	Forbidden
$\Gamma_{15}\rightarrow\Gamma_{25'}$		$\Lambda_{3'}\rightarrow\Lambda_1,\Lambda_3$	$\Lambda_{2'}\rightarrow\Lambda_1$	$X_{4'}\rightarrow X_5$	$X_{4'}\rightarrow X_5$	$X_{4'}\rightarrow X_3$	$\Delta_1\rightarrow\Delta_5$	$\Delta_5\rightarrow\Delta_5$	$\Delta_1\rightarrow\Delta_{2'}$
$\Delta_5\rightarrow\Delta_{2'}$	$\Delta_1\rightarrow\Delta_{2'}$	$\Lambda_{2'}\rightarrow\Lambda_3$	$\Lambda_{3'}\rightarrow\Lambda_3$	$X_{5'}\rightarrow X_3$	$X_{5'}\rightarrow X_5$		$\Delta_5\rightarrow\Delta_{2'}$		
$\Delta_5\rightarrow\Delta_5$		$\delta_1\rightarrow\delta_1,\delta_2$	$\delta_1\rightarrow\delta_1$	$\Delta_5\rightarrow\Delta_{2'}$	$\Delta_5\rightarrow\Delta_5$	$\Delta_1\rightarrow\Delta_{2'}$			
$X_{5'}\rightarrow X_3$	$X_{4'}\rightarrow X_3$	$\delta_2\rightarrow\delta_1,\delta_2$	$\delta_2\rightarrow\delta_2$	$\delta_1\rightarrow\delta_4$	$\delta_1\rightarrow\delta_3$	$\delta_1\rightarrow\delta_2$	$\delta_1\rightarrow\delta_1,\delta_2$	$\delta_1\rightarrow\delta_1$	
		$\chi_{2'}\rightarrow\chi_1$	$\chi_{2'}\rightarrow\chi_1$	$\delta_3\rightarrow\delta_2,\delta_3$	$\delta_4\rightarrow\delta_2$	$\delta_3\rightarrow\delta_4$	$\delta_2\rightarrow\delta_1,\delta_2$	$\delta_2\rightarrow\delta_2$	
		$\chi_{1'}\rightarrow\chi_1$		$\delta_4\rightarrow\delta_4$		$\delta_4\rightarrow\delta_3$			
				$\chi_{4'}\rightarrow\chi_2$	$\chi_{3'}\rightarrow\chi_2$	$\chi_{2'}\rightarrow\chi_2$	$\chi_1\rightarrow\chi_3$	$\chi_3\rightarrow\chi_3$	$\chi_4\rightarrow\chi_3$

dielectric properties of $SrTiO_3$, we expect, at most, one S state of non-negligible binding in the Wannier model. Such a state, if it exists at all, will not alter the interband selection rules. The possibility of a deeply bound Frenkel exciton cannot be ruled out *a priori*, but the observation[10] of photoconductivity associated with the fundamental absorption at 4°K, eliminates this interpretation. A brief discussion of Wannier exciton binding in $SrTiO_3$ is given in Appendix B. The notation employed to label the energy bands is explained in Appendix A.

II. BAND STRUCTURE AND OPTICAL SELECTION RULES

A. Cubic System

Our starting point is the band-structure calculation of cubic $SrTiO_3$ by Kahn and Leyendecker.[4] Their results, obtained with neglect of spin-orbit (SO) interaction, are schematized in Fig. 1 for wave vector $\mathbf{k}$ along the [100] direction. Electric-dipole selection rules for direct transitions are given in Table I(a). An example of an indirect transition will be discussed in Sec. III. The relatively weak SO splittings and their effects on the selection rules are summarized in Table II(a). As noted earlier, the conduction-band minima lie along ⟨100⟩, probably at X, a conclusion of the theory verified by the experiments of Frederikse *et al.*[5] The stationary point at Γ in the conduction band is believed to lie at most a few tenths of an eV above the minima.[4] The position of the valence-band maximum is less certain with $\mathbf{k}=0$ a probable candidate. However, the bands labeled Δ_1 and Δ_5 in Fig. 1 are relatively flat (even their order is not known with absolute confidence[4]), and a set of maxima at X, or along Δ, cannot be ruled out on the basis of present evidence. An additional possibility of valence-band maxima at the corners of the Brillouin zone[4] will not be considered here.

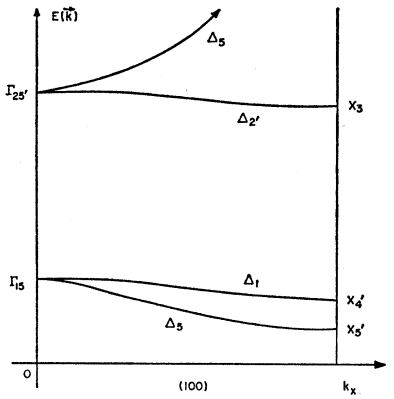

FIG. 1. Schematic of the band energies, $E(\mathbf{k})$, in $SrTiO_3$ for the cubic phase. Results are taken from Ref. 4. The wave vector $\mathbf{k}$ is along the [100] cubic axis. The notations Γ_i, X_i, and Δ_i are standard (see Refs. 4 and 25).

[10] L. H. Grabner (private communication). See also Ref. 9.

Below about 110°K, $SrTiO_3$ is no longer cubic, entering a tetragonal phase with additional phase transitions occurring as the temperature is lowered further.[11,12] However, Lytle[12] has shown via x-ray measurements that the deviation of the c/a ratio from unity is 5.6×10^{-4} in the tetragonal phase with deviations from cubicity of the same order in the lower temperature phases. Thus, naturally occurring deviations from the cubic band structure ought to be small compared with strains attainable with applied stress at low temperatures. Nevertheless, we consider experimental examination of the absorption edge of a single domain of natural crystals with polarized light to be worthwhile.

The SO splitting of the $\Gamma_{25'}$ conduction band (titanium d orbitals) has been estimated by Kahn[13] to be ~0.03 eV, with an even smaller SO splitting (~0.008 eV) expected for the Γ_{15} valence state (oxygen p orbitals). Hence, throughout, in using the selection rules in Table II, the listed orbital parentage of the levels is important, whenever a transition is given as allowed, especially away from $\mathbf{k}=0$, and where the SO interaction does not lift degeneracy. For example, for the cubic case along Δ [see Fig. 1], the optical transition $\Delta_6(\Delta_1)\rightarrow\Delta_7(\Delta_{2'})$ is allowed [Table II(a)], but *only weakly* via the SO interaction, since $\Delta_1\rightarrow\Delta_{2'}$ is forbidden [Table I(a)].

[11] R. O. Bell and G. Rupprecht, Phys. Rev. **129**, 90 (1963).
[12] F. W. Lytle, J. Appl. Phys. **35**, 2212 (1964).
[13] A. H. Kahn (private communication). See also A. H. Kahn, H. P. R. Frederikse, and J. H. Becker, in *Transition Metal Compounds: Transport and Magnetic Properties*, Informal Proceedings of the Buhl International Conference on Materials, Pittsburgh, 1963, edited by E. R. Schatz (Gordon and Breach Science Publishers, New York, 1964), p. 53.

TABLE II. Effects of spin-orbit coupling on the bands and optical transitions. Results are given for the cubic crystal, for [111] and [001] uniaxial stress, and for a static electric field along the [001] axis. The parentage tables give the band splittings due to spin-orbit effects. Representations collected in parentheses stick together due to time-reversal symmetry, e.g., $(\Lambda_5^{(-)}+\Lambda_6^{(-)})$. Notation: **E**=radiation electric field, c=axis of stress or static field, $A\perp$ ($A\parallel$)=allowed for $\mathbf{E}\perp c$ ($\mathbf{E}\parallel c$), F=forbidden. The representations, Γ_i, X_i, and Δ_i of the double group are in standard notation (see Refs. 25 and 26). The remainder follow from the single-group representations defined in Appendix A.

Orbital parentage	Optical transitions
(a) Cubic	
$\Gamma_{15}\rightarrow\Gamma_6^{(-)}+\Gamma_8^{(-)}$, $\Gamma_{25'}\rightarrow\Gamma_7^{(+)}+\Gamma_8^{(+)}$	$\Gamma_6^{(-)}\rightarrow\Gamma_8^{(+)}(A)$, $\Gamma_6^{(-)}\rightarrow\Gamma_7^{(+)}(F)$ $\Gamma_8^{(-)}\rightarrow\Gamma_7^{(+)}$, $\Gamma_8^{(+)}(A)$
$\Delta_5\rightarrow\Delta_6+\Delta_7$, $\Delta_{2'}\rightarrow\Delta_7$	$\Delta_6\rightarrow\Delta_6$, $\Delta_7(A)$, $\Delta_7\rightarrow\Delta_6$, $\Delta_7(A)$
$\Delta_1\rightarrow\Delta_6$	
$X_{4'}\rightarrow X_6^{(-)}$, $X_{5'}\rightarrow X_6^{(-)}+X_7^{(-)}$	$X_6^{(-)}\rightarrow X_7^{(+)}(A)$, $X_7^{(-)}\rightarrow X_7^{(+)}(A)$
$X_3\rightarrow X_7^{(+)}$, $X_5\rightarrow X_6^{(+)}+X_7^{(+)}$	
(b) [111] Stress	
$\Lambda_{3'}\rightarrow\Lambda_4^{(-)}+(\Lambda_5^{(-)}+\Lambda_6^{(-)})$	$\Lambda_4^{(-)}\rightarrow\Lambda_4^{(+)}$, $(\Lambda_5^{(+)}+\Lambda_6^{(+)})(A\perp)$
$\Lambda_{2'}\rightarrow\Lambda_4^{(-)}$, $\Lambda_1\rightarrow\Lambda_4^{(+)}$	$(\Lambda_5^{(-)}+\Lambda_6^{(-)})\rightarrow\Lambda_4^{(+)}(A\perp)$
$\Lambda_3\rightarrow\Lambda_4^{(+)}+(\Lambda_5^{(+)}+\Lambda_6^{(+)})$	$\Lambda_4^{(-)}\rightarrow\Lambda_4^{(+)}(A\parallel)$
	$(\Lambda_5^{(-)}+\Lambda_6^{(-)})\rightarrow(\Lambda_5^{(+)}+\Lambda_6^{(+)})(A\parallel)$
$\delta_i\rightarrow(\delta_3+\delta_4)$	$(\delta_3+\delta_4)\rightarrow(\delta_3+\delta_4)(A\perp,\parallel)$
$\chi_{i'}\rightarrow(\chi_3^{(-)}+\chi_4^{(-)})$, $\chi_i\rightarrow(\chi_3^{(+)}+\chi_4^{(+)})$	$(\chi_3^{(-)}+\chi_4^{(-)})\rightarrow(\chi_3^{(+)}+\chi_4^{(+)})(A\perp,\parallel)$
(c) [001] Stress	
At X, same as cubic case (a)	$X_6^{(-)}\rightarrow X_6^{(+)}$, $X_7^{(+)}(A\perp)$ $X_7^{(-)}\rightarrow X_6^{(+)}$, $X_7^{(+)}(A\perp)$ $X_6^{(-)}\rightarrow X_6^{(+)}(A\parallel)$, $X_7^{(-)}\rightarrow X_7^{(+)}(A\parallel)$
Along Δ, same as cubic case (a)	$\Delta_6\rightarrow\Delta_6$, $\Delta_7(A\perp)$, $\Delta_6\rightarrow\Delta_6(A\parallel)$ $\Delta_7\rightarrow\Delta_6$, $\Delta_7(A\perp)$, $\Delta_7\rightarrow\Delta_7(A\parallel)$
$\delta_i\rightarrow\delta_5$	$\delta_5\rightarrow\delta_5(A\perp,\parallel)$
$\chi_{i'}\rightarrow\chi_5^{(-)}$, $\chi_i\rightarrow\chi_5^{(+)}$	$\chi_5^{(-)}\rightarrow\chi_5^{(+)}(A\perp,\parallel)$
(d) [001] Static electric field	
Along Δ, same as cubic case (a)	Along Δ, same as [001] stress (c)
$\delta_i\rightarrow\delta_3+\delta_4$	$\delta_3\rightarrow\delta_3$, $\delta_4(A\perp)$, $\delta_3\rightarrow\delta_3(A\parallel)$ $\delta_4\rightarrow\delta_3$, $\delta_4(A\perp)$, $\delta_4\rightarrow\delta_4(A\parallel)$
$\chi_i\rightarrow\chi_5$	$\chi_5\rightarrow\chi_5(A\perp,\parallel)$

We emphasize that, neglecting SO effects, the direct transitions requiring minimum photon energy ($\Delta_1\rightarrow\Delta_{2'}$, $X_{4'}\rightarrow X_3$) are forbidden everywhere along the cubic axes except at $\Gamma(\Gamma_{15}\rightarrow\Gamma_{25'}$ is allowed). We shall return to this point in Sec. III.

B. Applied Stress and Static Electric Field

1. Uniaxial stress along [111] direction. The distorted lattice is rhombohedral. All valleys are displaced equivalently. Hence, only intravalley splittings occur. To achieve correspondence with the cubic band structure, we use a distorted cubic Brillouin zone instead of the reduced zone for a rhombohedral lattice. The perturbed bands are shown in Fig. 2, plotted along the distorted [100] cube axis k_x'. Optical selection rules, neglecting SO effects, are given in Table I(b) for radiation polarized $\perp c$, $\parallel c$, where c denotes the axis of applied stress. The cubic parentages of the levels are listed in Table III(a). As in the case of including SO effects, discussed

TABLE III. Parentage of the levels. The origins of the various levels in terms of the levels of the cubic system are given. **k** is the electron wave vector.

(a) [111] Stress		(b) [001] Stress		(c) [001] Static electric field	
k=0	**k** along [100]	**k**=0 or along [001]	**k** along [100]	**k**=0 or along [001]	**k** along [100]
$\Gamma_{15}\rightarrow\Lambda_{2'}+\Lambda_{3'}$	$\Delta_5\rightarrow\delta_1+\delta_2$	$\Gamma_{15}\rightarrow X_{5'}+X_{4'}$	$\Delta_1\rightarrow\delta_1$	$\Gamma_{15}\rightarrow\Delta_1+\Delta_5$	$\Delta_1\rightarrow\delta_1$
$\Gamma_{25'}\rightarrow\Lambda_1+\Lambda_3$	$\Delta_1\rightarrow\delta_1$	$\Gamma_{25'}\rightarrow X_5+X_3$	$\Delta_{2'}\rightarrow\delta_2$	$\Gamma_{25'}\rightarrow\Delta_{2'}+\Delta_5$	$\Delta_{2'}\rightarrow\delta_2$
	$\Delta_{2'}\rightarrow\delta_1$	$\Delta_i\rightarrow\Delta_i$	$\Delta_5\rightarrow\delta_3+\delta_4$	$\Delta_i\rightarrow\Delta_i$	$\Delta_5\rightarrow\delta_1+\delta_2$
	$X_{5'}\rightarrow\chi_1+\chi_2'$	$X_i\rightarrow X_i$	$X_3\rightarrow\chi_3$	$X_3\rightarrow\Delta_{2'}$	$X_3\rightarrow\chi_3$
	$X_{4'}\rightarrow\chi_{2'}$		$X_{4'}\rightarrow\chi_{2'}$	$X_{4'}\rightarrow\Delta_1$	$X_{4'}\rightarrow\chi_4$
	$X_3\rightarrow\chi_1$		$X_{5'}\rightarrow\chi_{3'}+\chi_{4'}$	$X_{5'}\rightarrow\Delta_5$	$X_{5'}\rightarrow\chi_1+\chi_3$

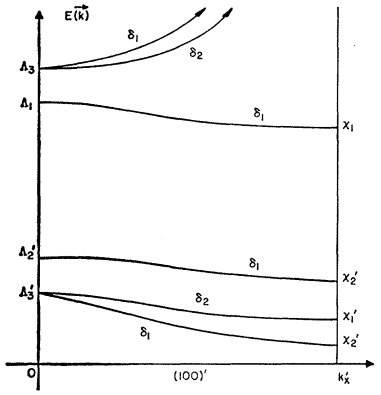

FIG. 2. Effects of applied stress along the [111] axis. k_x' is the distorted [100] axis. $E(\mathbf{k})$ denotes the band energies. Results are schematic with splittings exaggerated for clarity. Character tables for the representations Λ_i, δ_i, and χ_i are given in Tables IV and V.

earlier, the parentage is important for distinguishing between weakly and strongly allowed transitions for sufficiently weak applied stresses (which may include the strongest practicably attainable). For example, the minimal energy direct transition at $\chi, \chi_{2'}(X_{4'}) \rightarrow \chi_1(X_3)$, listed as allowed for both polarizations in Table I(b), is only weakly allowed since the transition $X_{4'} \rightarrow X_3$ is for bidden for the unstrained crystal. Effects of SO interaction are given in Table II(b).

2. Uniaxial stress along the [001] direction. The strained lattice is tetragonal (D_{4h} symmetry). The valleys along the [100] and [010] axes, i.e., $\perp c$ (the axis of strain), move differently from those along [001]. The former are subject to intravelley splitting whereas the latter are not. The perturbed bands are shown in Fig. 3(a) for $\mathbf{k} \perp c$ and in Fig. 3(b) for $\mathbf{k} \| c$. Selection rules for polarized radiation are listed in Table I(c); cubic parentages of the levels, in Table III(b); and effects of SO interaction, in Table II(c).

3 Static electric field along the [001] direction. In addition to the usual Franz-Keldysh[14] effect, we expect nontrivial Stark shifts and splittings of the bands to occur.[15] Our reasoning is based upon the fact that $SrTiO_3$ is nearly a ferroelectric. Weaver[16] has found a Curie-Weiss behavior for the static dielectric constant ϵ_0 over a range of temperatures from room temperature ($\epsilon_0 \sim 300$) to 60°K ($\epsilon_0 \sim 3000$). At 1.4°K, $\epsilon_0 \sim 2 \times 10^4$, a saturation value. Moreover, infrared measurements of Barker and Tinkham[17] and neutron work of Cowley[18] demonstrate that the lowest transverse optical (TO) mode frequency decreases with temperature in accord with Cochran's theory[19] of ferroelectrics. Associated with this soft TO mode [we estimate $(\hbar\omega_{TO}/k) \sim 10$°K at helium temperature], one expects large ionic displacements with applied electric field, at least at low temperatures. Thus, the crystal potential should be altered considerably with field. Accordingly, we have assumed the symmetry, C_{4v} for $SrTiO_3$ with applied [001] field at low temperatures. Additional effects associated with nonperiodicity due to the field appear in the Franz–Keldysh mechanism. Our assumption is strengthened somewhat by the observations of Harbeke[20] on the ferroelectric, SbSI. He found large frequency shifts of the fundamental edge with applied field, both above and below the Curie temperature, in a direction opposite to that expected on the basis of the Franz–Keldysh mechanism alone. Moreover, we note that lack of inversion symmetry in $SrTiO_3$ with applied field is implied by the work of Winter and Rupprecht,[21] who found piezoelectricity below 40°K, provided that a small bias field was applied. (Inversion is not in the group, C_{4v}.) Despite these favorable indications, our assumption of C_{4v} symmetry remains somewhat tenuous. Note, however, that the symmetry of $BaTiO_3$ is known to be C_{4v} in the tetragonal ferroelectric phase, where optical dichroism in the fundamental absorption has been observed by Casella and Keller.[22] Moreover, Cardona[8] has shown that the reflection spectra of $BaTiO_3$ and $SrTiO_3$ are quite similar, a fact we shall exploit in Sec. III.

The energy bands are pictured in Fig. 4(a) for $\mathbf{k}$ along [100] and in Fig. 4(b) for $\mathbf{k}$ along [001], the field direction. Dipole selection rules and cubic parentages, neglecting SO interaction, are given in Table I(d) and Table III(c), respectively. SO effects are stated in Table II(d).

III. TWO MODELS

We discuss two examples of the application of the results given in Sec. II, which are of practical interest.

1. Present band model. For the cubic case, the transitions $\Delta_1 \rightarrow \Delta_{2'}$ and $X_{4'} \rightarrow X_3$ are forbidden, as noted earlier. Only the transition $\Gamma_{15} \rightarrow \Gamma_{25'}$ is allowed between the highest valence band and the conduction band everywhere along the [100] axis. Since the conduction minima lie away from Γ, we would have indirect transitions of the type $\Gamma_{15} \rightarrow \Gamma_{25'}$ (virtual) $\rightarrow X_3$, where the last step proceeds via phonon emission and absorption. In the following we consider only the first step of this process. Applying [111] stress the $\Lambda_{2'} \rightarrow \Lambda_1$ transition, allowed for $\mathbf{E} \| c$, should dominate [see Fig. 2]. For [001] stress, $X_{4'} \rightarrow X_3$ is forbidden and, at shorter wavelengths, either $X_{5'} \rightarrow X_3$ ($\mathbf{E} \perp c$) or $X_{4'} \rightarrow X_5$ ($\mathbf{E} \perp, \| c$) should occur at $\mathbf{k}=0$. Finally, with a static field applied

[14] W. Franz, Z. Naturforsch. **13**, 484 (1958); L. V. Keldysh, Zh. Eksperim. i Teor. Fiz. **34**, 1138 (1958) [English transl.: Soviet Phys.—JETP **7**, 788 (1958)].

[15] For a detailed discussion of effects on the absorption coefficient, see J. Calloway, Phys. Rev. **130**, 549 (1963); **134**, A998 (1964); K. Tharmalingam, *ibid.* **130**, 2204 (1963); C. B. Duke, Phys. Rev. Letters **15**, 625 (1965); D. G. Thomas and J. J. Hopfield, Phys. Rev. **124**, 657 (1962).

[16] H. E. Weaver, J. Phys. Chem. Solids **11**, 274 (1959).

[17] A. S. Barker, Jr., and M. Tinkham, Phys. Rev. **125**, 1527 (1962).

[18] R. A. Cowley, Phys. Rev. **134**, A981 (1964).

[19] W. Cochran, Advan. Phys. **9**, 387 (1960).

[20] G. Harbeke, J. Phys. Chem. Solids **24**, 957 (1963).

[21] W. H. Winter and G. Rupprecht, Bull. Am. Phys. Soc. **7**, 438 (1962).

[22] R. C. Casella and S. P. Keller, Phys. Rev. **116**, 1469 (1959). See also A. Frova and P. J. Broddy, Phys. Rev. Letters **16**, 688 (1966).

along [001] we have $\Delta_1 \rightarrow \Delta_{2'}$ forbidden, with the allowed transition at $\mathbf{k}=0$ stemming from either $\Delta_5 \rightarrow \Delta_{2'}$ ($\mathbf{E}\perp c$) or $\Delta_1 \rightarrow \Delta_5$ ($\mathbf{E}\perp c$). Including SO effects, a weak $\mathbf{k}=0$ transition $X_6^-(X_{4'}) \rightarrow X_7^+(X_3)$ ($\mathbf{E}\perp c$) might be observable on the low energy side of the strongly allowed transition for the case of [001] strain. The same applies to the weak $\mathbf{k}=0$ transition, $\Delta_6(\Delta_1) \rightarrow \Delta_7(\Delta_{2'})$, ($\mathbf{E}\perp c$) with applied [001] field.

Since the energy separation between the $\Gamma_{25'}$ stationary point and the ⟨100⟩ minima for the cubic crystal is presumably small, one would expect a noticeable change in the absorption curves as the photon energy increases to the point that (real) direct transitions can occur at $\mathbf{k}=0$, this, despite the complications associated with the many-phonon Urbach process.[23] No such change has been observed by Blunt and Cohen.[9] It will be interesting to see what happens should transmission data on thin films of $SrTiO_3$ become available.

2. Model with modified valence bands. The reflection spectra of Cardona[8] imply a strong similarity between the band structures of $SrTiO_3$ and $BaTiO_3$. Since the latter has C_{4v} symmetry in the tetragonal ferroelectric phase, the band structure we have obtained for $SrTiO_3$ with electric field along [001] [Fig. 4(a,b)] ought to be useful in interpreting the dichroic fundamental absorption of $BaTiO_3$ reported by Casella and Keller.[22] With polarized light they found two absorption edges separated by about 0.05 eV at the frequency of maximum dichroism (3.21 eV at room temperature). The edge active for $\mathbf{E}\perp c$ occurs at lower photon energy. Lacking detailed knowledge of the possible band symmetries, the data were interpreted by these authors in terms of a general selection rule[24] which had, in fact, predicted the sign of the dichroic shift correctly prior to measurement. Given our present results, the $BaTiO_3$ data at the fundamental edge can perhaps be understood best by reversing the order of the valence bands Δ_1 and Δ_5 in Fig. 4(b) with a consequent shift of levels in Fig. 4(a). (Note that the transitions $\Delta_1 \rightarrow \Delta_{2'}$, $\chi_4 \rightarrow \chi_3$ are forbidden.) Because of compatibility and $\delta_1-\delta_1$ repulsion, the revised order of the valence bands at χ becomes $\chi_1>\chi_3>\chi_4$, where we have used the symmetry type of denote the associated energy in the inequalities. For $\mathbf{k}$ along [100], the direct transitions from the (revised) upper valence band ($\Delta_5-\delta_1-\chi_1$) to the (unchanged) conduction band ($\Delta_{2'}-\delta_2-\chi_3$) are everywhere allowed ($\mathbf{E}\perp c$). Transitions from the next lower valence band ($\Delta_5-\delta_2-\chi_3$), which splits off away from $\mathbf{k}=0$, are as follows: $\chi_3 \rightarrow \chi_3$ ($\mathbf{E}\|c$), $\delta_2 \rightarrow \delta_2$ ($\mathbf{E}\perp,\|c$). The results are consistent with the observations reported in Ref. 22. At $\mathbf{k}=0$ and along [001] it may be necessary to include the weak SO effects, since they lift degeneracy. Δ_5 splits into $\Delta_6+\Delta_7$ with Δ_6 expected higher because of $\Delta_6-\Delta_6$ repulsion from the (revised) lower $\Delta_6(\Delta_1)$ band. Thus, along Δ, the lowest energy transition is $\Delta_6(\Delta_5) \rightarrow \Delta_7(\Delta_{2'})$, ($\mathbf{E}\perp c$), followed by $\Delta_7(\Delta_5) \rightarrow \Delta_7(\Delta_{2'})$, ($\mathbf{E}\perp,\|c$), again consistent with the observations in Ref. 22. [Since the observed dichroic splitting (~0.05 eV) is about six times larger than the expected SO effect (~0.008 eV) one is tempted to believe that the transition is direct and occurs at the zone face, i.e., is the process $\chi_1 \rightarrow \chi_3$. The following analysis, however, does not depend upon this detailed assumption, and other possibilities are considered.]

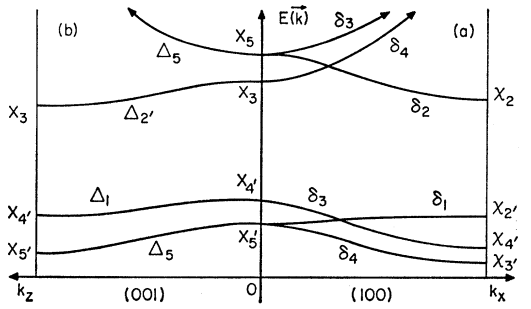

FIG. 3. Effects of uniaxial stress along the [001] axis. (a) $\mathbf{k}$ along [100], $\perp$ stress, (b) $\mathbf{k}$ along [001], $\|$ stress. $E(\mathbf{k})$ denotes the band energies. The notations X_i and Δ_i are standard (see Ref. 25). Character tables for the representations χ_i and δ_i are given in Table VI.

Turning the argument around, we assume the same reversal of levels occurs for $SrTiO_3$ in electric field. Comparing Fig. 1 with Fig. 4(b), or tracing through the cubic parentages [Table III(c)] leads naturally to the assumption that the order of the valence bands Δ_1 and Δ_5 (hence, also $X_{4'}$ and $X_{5'}$) should be reversed for cubic $SrTiO_3$. As noted earlier, reversing the order of these levels is possible within the limits of accuracy of the calculation of Kahn and Leyendecker.[4] [In contrast, for the conduction band, because of an approximate symmetry condition, they can predict firmly that the band ($\Gamma_{25'}-\Delta_{2'}-X_3$) lies lowest.] Moreover, inverting the order of $X_{4'}$ and $X_{5'}$ does not affect Cardona's[8] interpretation of the strong peaks labeled A_1(3.8 eV) and A_2(4.5 eV).

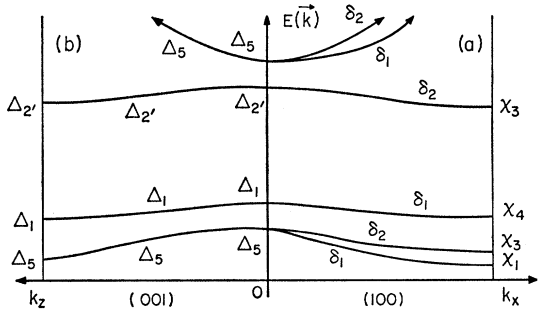

FIG. 4. Effects of static electric field along the [001] axis. (a) $\mathbf{k}$ along [100], $\perp$ field, (b) $\mathbf{k}$ along [001], $\|$ field. The notation Δ_i is standard (see Ref. 25). Character tables for δ_i and χ_i are given in Tables V and VI.

[23] A theoretical analysis of the "direct" Urbach process has been given by Mahan, who obtains the electron spectral density at $\mathbf{k}=0$ in the presence of many-phonon processes [G. D. Mahan, Phys. Rev. **145**, 602 (1966)].

[24] See also R. C. Casella, Phys. Rev. **114**, 1514 (1959).

Knowing the cubic parentages [Table III], it is easy to construct a plausible revised band picture similar to those shown in Figs. 1–4 for the remaining cases of [111] and [001] stresses: For [111] stress,

$$(\chi_{2'}-\delta_1-\Lambda_{3'})\geq(\chi_{1'}-\delta_2-\Lambda_{3'})>(\chi_{2'}-\delta_1-\Lambda_{2'}), \quad (1)$$

where the equality holds at $\mathbf{k}=0$, where the two bands touch. For [001] stress,

$$\begin{aligned}&(X_{5'}-\Delta_5-X_{5'})>(X_{4'}-\Delta_1-X_{4'}), \quad \mathbf{k}\|[001];\\ &(X_{5'}-\delta_4-\chi_{3'})\geq(X_{5'}-\delta_1-\chi_{2'}),\\ &(X_{5'}-\delta_4-\chi_{3'})>(X_{4'}-\delta_3-\chi_{4'}), \quad \mathbf{k}\|[100].\end{aligned} \quad (2)$$

For $\mathbf{k}$ along [100], the bands $(X_{5'}-\delta_1-\chi_{2'})$ and $(X_{4'}-\delta_3-\chi_{4'})$ cross with $X_{5'}>X_{4'}$ at $\mathbf{k}=0$ and $\chi_{4'}>\chi_{2'}$ at the zone boundary. In all cases the conduction bands are as given in Figs. 1–4.

An important prediction of the model is that in the presence of a static electric field along [001] and at low temperatures, $SrTiO_3$ should exhibit a dichroic fundamental absorption closely resembling that observed[22] in $BaTiO_3$, a prediction going beyond the broad similarity observed by Cardona.[8] The experiment may be difficult, since transmission measurements should be made on a single domain. Another test involves the [111]-stressed crystal, assuming the $\mathbf{k}=0$ (virtual) transition dominates the (possibly indirect) process. According to the present model the (first step of the indirect) transition is $\Lambda_{3'}\rightarrow\Lambda_1$ ($\mathbf{E}\perp c$), whereas in the previous model we have $\Lambda_{2'}\rightarrow\Lambda_1$ ($\mathbf{E}\|c$). However, this prediction is complicated by the weak SO interaction, which lifts the $\Lambda_{3'}$ degeneracy admitting a process allowed with both polarizations at longer wavelength. Varying the amount of stress might help sort out the effects. Depending upon the initial assumptions which future experiments might imply, other criteria can be worked out readily from the tables.

Should the second model survive, the application of a strong [001] stress might enable one to decide how the valleys move in the experiments of Schooley[1] and of Tufte and Stelzer.[6] It predicts that valleys along [100] and [010] admit a transition $\chi_{3'}\rightarrow\chi_2$ ($\mathbf{E}\|c$), whereas for the valley along [001] the allowed process is $X_{5'}\rightarrow X_3$ ($\mathbf{E}\perp c$). (The latter process also applies to the $\mathbf{k}=0$ transition.) Unlike the case of [111] stress, discussed above, SO effects, which lift the $X_{5'}$ degeneracy, are not expected to affect this conclusion, because the SO-induced allowed component with $E\|c$ should lie at shorter wavelength.

IV. SUMMARY AND CONCLUSIONS

Starting with the present (incomplete) knowledge of the energy band structure of $SrTiO_3$, we have determined the effects of applied uniaxial stress and static electric field on the bands, and derived selection rules for polarized optical transitions in the region of the fundamental absorption of the perturbed crystals. We have considered only interband transitions, but possible exciton formation, believed unlikely, does not alter our conclusions, since only S states could be sustained (Appendix B). The results of the symmetry analysis were applied to two models in Sec. III. In the presence of a strong electric field along, say, the [001] axis, we assume $SrTiO_3$ has C_{4v} symmetry, the known symmetry of $BaTiO_3$ in the ferroelectric state, for which optical transmission data at the dichroic fundamental edge exist. Utilizing the established broad similarity between the reflection spectra of $SrTiO_3$ and $BaTiO_3$ as well as the $SrTiO_3$ band calculation, we were led to a model for $BaTiO_3$ which, working backwards, suggests that the valence band $(\Gamma_{15}-\Delta_5-X_{5'})$ lies energetically above the band $(\Gamma_{15}-\Delta_1-X_{4'})$ in $SrTiO_3$. This order is opposite to that resulting from the prior calculation, but lies within its limits of probable error and is not inconsistent with known data. The lowest conduction band, which the earlier calculation predicts with confidence to be $(\Gamma_{25'}-\Delta_{2'}-X_3)$, is left unaltered. We called this model 2, model 1 being that with the valence bands in the order predicted originally.

Model 2 implies that the edge absorption of $SrTiO_3$ at low temperatures with [001] electric field should be dichroic in the same sense as $BaTiO_3$ ($\mathbf{E}\perp c$ at longer wavelength) a prediction which goes beyond the established broad similarity of the two structures. Also, it predicts that under [111] stress the first allowed transition mode is with $\mathbf{E}\perp c$, the stress axis, whereas model 1 yields a lowest energy transition for $\mathbf{E}\|c$. However, this test is subject to qualifications (Sec. III). Model 1 is characterized by the existence of weakly allowed, long-wavelength precursors to the allowed transitions for the perturbed bands, stemming from forbidden transitions in the cubic band structure. Should model 2 prove correct, it provides a means of obtaining information on how the valleys move with stress, useful from the point of view of the superconductivity experiments which motivated this work. That is, for the case of [001] stress, the low energy transition is allowed with $\mathbf{E}\|c$ if the valleys which lie in directions $\perp c$ move to lower energies relative to the valleys oriented along c. If the valleys move oppositely to that described, the process with $\mathbf{E}\perp c$ occurs first.

ACKNOWLEDGMENTS

I wish to thank H. P. R. Frederikse, L. H. Grabner, and A. H. Kahn for informative discussions; R. F. Blunt, M. I. Cohen, and J. F. Schooley for permission to quote from their data prior to publication; and A. Feldman and R. A. Forman for calling my attention to two relevant experimental papers.

APPENDIX A. CHARACTER TABLES NEGLECTING SPIN-ORBIT INTERACTIONS

1. The notations Γ, X, and Δ (see Fig. 1) are standard and the tables may be found in the paper of Bouckaert,

TABLE IV. Character table, $\mathbf{k}=0$, for [111] stress.

	E	$3C_2$	$2C_3$
Λ_1	1	1	1
Λ_2	1	−1	1
Λ_3	2	0	−1

Smoluchowski, and Wigner.[25] The double-group representations are given in the work of Elliott.[26]

2. [111] stress. At $\Lambda(\mathbf{k}=0)$ and at χ (the displaced X point of the cubic Brillouin zone) the parity operation is in the little group, $G^{\mathbf{k}}$. Primed (unprimed) representations in Fig. 2 are odd (even) under space inversion J. We give only representations of the factor group of

TABLE V. Character table, $\mathbf{k}$ along [100] for [111] stress.

χ / δ	E / E	C_2 / JC_2
χ_1, δ_1	1	1
χ_2, δ_2	1	−1

proper rotations. At δ, $G^{\mathbf{k}}$ consists of only the identity and a reflection plane. See Tables IV and V.

3. [001] stress. At χ, the center of the (100) face of the zone, parity is in $G^{\mathbf{k}}$. We give only representations of the proper subgroup using primes in Fig. 3 to denote odd-parity representations of the full group, as in the case of the [111] stress, treated above. The full group along δ is given. See Table VI.

TABLE VI. Character table, $\mathbf{k}$ along [100] for [001] stress.

χ / δ	E / E	$C_2\|\|$ / $C_2\|\|$	$C_2\perp$ / $JC_2\perp$	C_4^2 / JC_4^2
χ_1, δ_1	1	1	1	1
χ_2, δ_2	1	1	−1	−1
χ_3, δ_3	1	−1	1	−1
χ_4, δ_4	1	−1	−1	1

4. [001] electric field. At χ, parity is not in $G^{\mathbf{k}}$. The representations χ_i of $G^{\mathbf{k}}$ are given by the proper factor group representations at χ for the case of the [001] stress, given above, if one reads the sequence (E, C_4^2, $JC_2\|$, $JC_2\perp$) in place of the symbols in the row labeled χ in Table VI. Along δ, $G^{\mathbf{k}}=(E, JC_2\perp)$, and the representations are given in Table V.

APPENDIX B. EXCITON BINDING ENERGIES

Since the dielectric constant $\epsilon_0\simeq 2\times 10^4$ at 4°K, the hydrogenic binding energy $B\sim 4\times 10^{-8}$ eV, assuming a reduced mass $\mu\sim m$, the free electron mass.[5] At room temperature, $\epsilon_0\simeq 300$ and $B\sim 2\times 10^{-4}$ eV. Hence, in the simple hydrogenic model, exciton effects are wholly negligible at low temperatures and, because of thermal broadening, probably also at room temperature. Although the large static dielectric constant is of relevance in reducing the exciton binding energy, we do not take the above crude calculation seriously.

In an attempted refinement, we consider the Haken–Schottky[27] potential, $V(r)=-(e^2/r)\epsilon^{-1}(r)$, where $\epsilon(r)$ is their effective dielectric function, which we approximate further, writing

$$\epsilon^{-1}(r)=\epsilon_\infty^{-1}\exp(-r/\rho)+\epsilon_0^{-1}. \tag{B1}$$

In the above, $\epsilon_\infty=5.2$ is the high frequency dielectric constant and for simplicity we have set $m_e=m_h=2m$, where m_e and m_h are the electron and hole masses, respectively; $\rho=(\hbar/2m_e\omega_{LO})^{\frac{1}{2}}\simeq 4$ Å is a shielding parameter; ω_{LO} is the longitudinal optical phonon frequency, and we have used $\hbar\omega_{LO}\simeq 0.1$ eV.[28] Neglecting the term ϵ_0^{-1} in Eq. (B1) at low temperatures, we obtain a shielded potential, for which the author[29] has shown that a bound state exists provided that, in the present context, $\rho\geq 0.84a_\infty$. Here $a_\infty\equiv(\epsilon_\infty m/\mu)\times 0.59$ Å$\simeq 3$ Å is the exciton radius in the absence of ionic shielding; μ is the reduced mass. The analysis implies the existence of a bound S state, but (using an effective square-well approximation[30]) no bound states for $l\geq 1$. The use of an effective square-well potential to determine for exciton binding for an exponentially shielded potential is discussed in Ref. 29, where it is shown that the criterion for binding one obtains for a single S state is $\rho\geq 0.6a_\infty$ in the present notation, to be compared with $\rho\geq 0.84a_\infty$ which follows from the exponential. Therefore, considering the nature of the approximations involved in obtaining Eq. (B1) and in setting $m_h=m_e$, the simpler square-well approximation is considered adequate for investigating higher angular momentum states. We omit details, but refer to Refs. 29 and 30 and state the result. The condition for a single bound P state is $\rho\geq 2.5a_\infty$. Since $\rho/a_\infty=1.3$, this condition is not satisfied. Despite the approximate nature of our "refined" calculation, we do take seriously the absence of or negligible binding of exciton states with $l\geq 1$ in $SrTiO_3$, whence the selection rules for the transition to the (S state) exciton are the same as derived in the text, neglecting exciton effects. We remark that even the existence of an appreciably bound S state is suspect, since the potential is confined mostly to a single unit cell (the lattice constant $\simeq 3.9$ Å). Effective-mass theory and even the dielectric function have doubtful meaning over such small distance intervals.

[25] L. P. Bouckaert, R. Smoluchowski, and E. Wigner, Phys. Rev. **50**, 58 (1936).
[26] R. J. Elliott, Phys. Rev. **96**, 280 (1954).
[27] H. Haken and W. Schottky, Z. Physik. Chem. (Frankfurt) **16**, 218 (1958); See also the review by R. S. Knox, in *Solid State Physics*, edited by F. Seitz and D. Turnbull (Academic Press Inc., New York, 1963), Suppl. 5.
[28] See, for example, D. M. Eagles, J. Phys. Chem. Solids **26**, 672 (1965).
[29] R. C. Casella, J. Appl. Phys. **34**, 1703 (1963). The analysis employs the results of L. Hulthén and K. V. Laurikainen [Rev. Mod. Phys. **23**, 1 (1951)], who considered the Yukawa potential.
[30] See, for example, L. I. Schiff, *Quantum Mechanics* (McGraw-Hill Book Company, Inc., New York, 1949).